AIP Advances

Characterisation and optimisation of PECVD SiNx as an antireflection coating and passivation layer for silicon solar cells

Yimao Wan, Keith R. McIntosh, and Andrew F. Thomson

Citation: AIP Advances 3, 032113 (2013); doi: 10.1063/1.4795108
View online: http://dx.doi.org/10.1063/1.4795108
View Table of Contents: http://aipadvances.aip.org/resource/1/AAIDBI/v3/i3
Published by the American Institute of Physics.

Related Articles

Growth and band alignment of Bi2Se3 topological insulator on H-terminated Si(111) van der Waals surface
Appl. Phys. Lett. 102, 074106 (2013)

Effect of microwave plasma treatment on silicon dioxide films grown by atomic layer deposition at low temperature
J. Appl. Phys. 113, 064102 (2013)

Strain engineering in epitaxial La1−xSr1+xMnO4 thin films
J. Appl. Phys. 113, 053906 (2013)

Synthesis and characterization of MoS2/Ti composite coatings on Ti6Al4V prepared by laser cladding
AIP Advances 3, 022106 (2013)

Molecular beam epitaxy of high structural quality Bi2Se3 on lattice matched InP(111) substrates
Appl. Phys. Lett. 102, 041914 (2013)

Additional information on AIP Advances

Journal Homepage: http://aipadvances.aip.org
Journal Information: http://aipadvances.aip.org/about/journal
Top downloads: http://aipadvances.aip.org/most_downloaded
Information for Authors: http://aipadvances.aip.org/authors

ADVERTISEMENT

AIP Advances
Now Indexed in Thomson Reuters Databases
Explore AIP's open access journal:
- Rapid publication
- Article-level metrics
- Post-publication rating and commenting

Downloaded 05 Mar 2013 to 150.203.45.141. All article content, except where otherwise noted, is licensed under a Creative Commons Attribution 3.0 Unported license.
See: http://creativecommons.org/licenses/by/3.0/

AIP ADVANCES 3, 032113 (2013)

Characterisation and optimisation of PECVD SiN_x as an antireflection coating and passivation layer for silicon solar cells

Yimao Wan,[1] Keith R. McIntosh,[2] and Andrew F. Thomson[1]
[1]*Research School of Engineering, The Australian National University (ANU), Canberra ACT 0200, Australia*
[2]*PV Lighthouse, Coledale NSW 2515, Australia*

(Received 1 November 2012; accepted 14 February 2013; published online 5 March 2013)

In this work, we investigate how the film properties of silicon nitride (SiN_x) depend on its deposition conditions when formed by plasma enhanced chemical vapour deposition (PECVD). The examination is conducted with a Roth & Rau AK400 PECVD reactor, where the varied parameters are deposition temperature, pressure, gas flow ratio, total gas flow, microwave plasma power and radio-frequency bias voltage. The films are evaluated by Fourier transform infrared spectroscopy to determine structural properties, by spectrophotometry to determine optical properties, and by capacitance–voltage and photoconductance measurements to determine electronic properties. After reporting on the dependence of SiN_x properties on deposition parameters, we determine the optimized deposition conditions that attain low absorption and low recombination. On the basis of SiN_x growth models proposed in the literature and of our experimental results, we discuss how each process parameter affects the deposition rate and chemical bond density. We then focus on the effective surface recombination velocity S_{eff}, which is of primary importance to solar cells. We find that for the SiN_x prepared in this work, 1) S_{eff} does not correlate universally with the bulk structural and optical properties such as chemical bond densities and refractive index, and 2) S_{eff} depends primarily on the defect density at the SiN_x-Si interface rather than the insulator charge. Finally, employing the optimized deposition condition, we achieve a relatively constant and low $S_{eff,UL}$ on low-resistivity ($\leq$1.1 Ωcm) *p*- and *n*-type c-Si substrates over a broad range of n = 1.85–4.07. The results of this study demonstrate that the trade-off between optical transmission and surface passivation can be circumvented. Although we focus on photovoltaic applications, this study may be useful for any device for which it is desirable to maximize light transmission and surface passivation. *Copyright 2013 Author(s). This article is distributed under a Creative Commons Attribution 3.0 Unported License.* [http://dx.doi.org/10.1063/1.4795108]

I. INTRODUCTION

An antireflection coating (ARC) is an important feature of crystalline silicon solar cells. Ideally, this layer should not only maximize optical transmission but simultaneously suppress surface recombination. Amorphous hydrogenated silicon nitride a-SiN_x:H (hereafter referred to as SiN_x) synthesised by low-temperature PECVD has become the state-of-the-art ARC layer for c-Si solar cells to fulfil these two requirements.[1,2] It also provides a humidity barrier, protecting underlying interfaces from the degrading effects of moisture,[3,4] and is a source of hydrogen for passivating silicon bulk defects.[5–8]

On c-Si substrates, low surface recombination has been achieved by various plasma techniques and gas mixtures.[9–15] Details of the deposition processes and silicon substrates employed in these studies are included in Table I. Figure 1 summarizes the results by plotting the upper limit to the

 © Author(s) 2013

Downloaded 05 Mar 2013 to 150.203.45.141. All article content, except where otherwise noted, is licensed under a Creative Commons Attribution 3.0 Unported license.
See: http://creativecommons.org/licenses/by/3.0/

TABLE I. Summary on the details of PECVD processes and silicon substrates employed in references.

PECVD process details[a]			Substrate[b] (FZ, {100} *p*-Si)		Lowest $S_{eff,UL}$ and associated *n*		
Technique	T (°C)	Reactant gas mixture	ρ_{bulk} ($\Omega \cdot$ cm)	W (μm)	$S_{eff,UL}$[e] (cm/s)	*n* at 632 nm	Refs.
Remote lab	375[c]	SiH_4, NH_3	1.50	300	11.5	2.4	9
Direct HF lab	350[d]	SiH_4, NH_3, diluted H_2	1.25	250	7.5	3.2	10
Remote inline	350[d]	SiH_4, NH_3, diluted H_2	1.50	300	10.3	2.7	11
Direct LF lab	370[d]	SiH_4, NH_3	5.00	300	13.5	3.0	12
Remote inline	450[d]	SiH_4, NH_3	1.50	280	5.9	2.5	13
Direct HF lab	400[d]	SiH_4, NH_3, diluted N_2	1.00	400	17.9	1.9	14
Dual-mode lab	290[c]	SiH_4, NH_3,Ar	0.85	300	1.6	1.9	15

[a]Process variable altered in Refs. 10–13 is gas flow ratio.
[b]FZ-float zone; ρ_{bulk}-nominal bulk resistivity; W-silicon substrate width.
[c]Measured temperature on substrate table by thermal coupler.
[d]Temperature setpoint.
[e]$S_{eff,UL}$ is cited at excess carrier density $\Delta n = 10^{15}$ cm^{-3} and recalculated using the latest Auger model.[16]

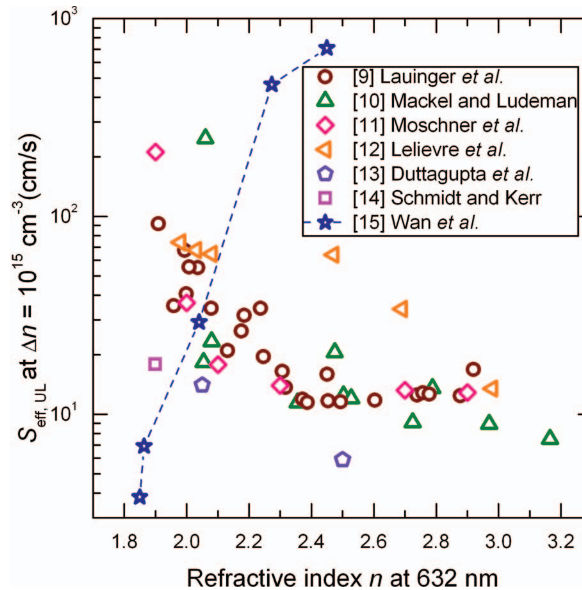

FIG. 1. The upper limit to the effective surface recombination velocity $S_{eff,UL}$ as a function of refractive index *n* at 632 nm for SiN_x-passivated FZ *p*-Si substrates. SiN_x is deposited by a variety of deposition techniques and gas mixtures as summarised in Table I. The dash-line highlights the opposing trend presented in Ref. 15.

effective surface recombination velocity $S_{eff,UL}$ as a function of the refractive index *n*. The presented $S_{eff,UL}$ and *n* are at an excess carrier density of $\Delta n = 10^{15}$ cm^{-3} and a wavelength of 632 nm, respectively. As can be seen, irrespective of deposition techniques and reactant gas mixtures employed in Refs. 10, 12, and 13 an apparent trend is observed: $S_{eff,UL}$ decreases as *n* increases. More complicated trends can be observed for the results in Refs. 9 and 11, whereby $S_{eff,UL}$ first decreases with increasing *n* and saturates for *n* above 2.3.

The results presented in Refs. 9–13 make it appear that the optimum surface passivation is acquired by Si-rich SiN_x of high *n*. Since high-*n* SiN_x is well-known to be highly absorbing of short wavelength light, this trend implies there is a trade-off between optical transmission and surface passivation. However, two previous studies suggest that the trade-off can be circumvented: Schmidt *et al.*[14] achieved a low $S_{eff,UL}$ (15.2 cm/s on FZ 1.0-$\Omega \cdot$ cm *p*-Si) using a stoichiometric SiN_x ($n = 1.9$) by including N_2 with SiH_4 and NH_3, and our recent work[15] presented a low $S_{eff,UL}$ (1.6 cm/s on FZ 0.85-$\Omega \cdot$ cm *p*-Si, and lower still on FZ 0.47-$\Omega \cdot$ cm *n*-Si) by low absorption SiN_x. The key process

Downloaded 05 Mar 2013 to 150.203.45.141. All article content, except where otherwise noted, is licensed under a Creative Commons Attribution 3.0 Unported license. See: http://creativecommons.org/licenses/by/3.0/

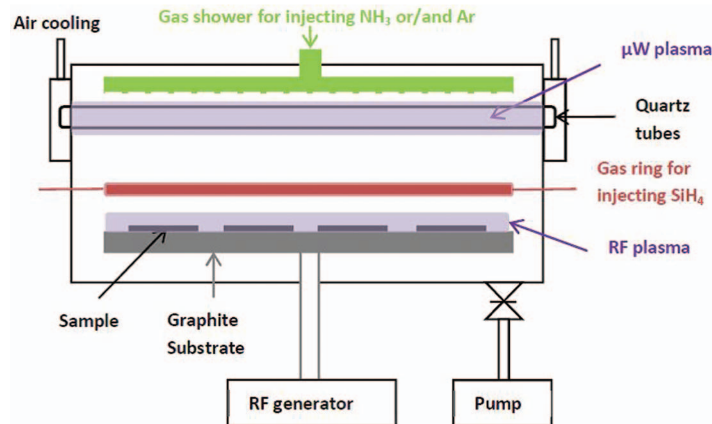

FIG. 2. Schematic cross section of a microwave/radio-frequency (μW/RF) PECVD reactor.

to obtain the film in Ref. 15 is by increasing the deposition pressure in a microwave/radio-frequency (μW/RF) PECVD reactor. These latter results are also included in Figure 1, showing that as the deposition pressure increases, both $S_{\mathrm{eff,UL}}$ and n decrease. This trend is opposite to the previously assumed trend, providing the opportunity to obtain low absorption and low recombination. The two works[14,15] show that remarkably low surface recombination is achievable by lowly absorbing SiN_x and imply that the trade-off between optical transmission and surface passivation can be circumvented.

In this paper, we first review the SiN_x deposition system employed in this work and the SiN_x growth mechanisms proposed in the literature. These are presented in Section II. We then conduct two experiments to characterise and optimise SiN_x as an ARC and passivation layer for solar cells. Section III presents the first experiment, which is a central composition experiment (CCE) that examines six deposition parameters. After reporting on the dependence of SiN_x properties (i.e. deposition rate, structural, optical and electronic properties) on the deposition parameters, we state the optimized deposition conditions that attain low absorption and low recombination. On the basis of the SiN_x growth mechanism described in Section II and of our experimental results, we then discuss how the deposition parameters affect the film properties. Further, we perform correlative studies to understand the relationships between various SiN_x properties. Section IV presents the second experiment in which the gas-flow rate is varied and the other depositions conditions are set to their optimal values. It demonstrates that a relatively constant and low $S_{\mathrm{eff,UL}}$ (< 10 cm/s) on low-resistivity ($\leq$1.1 Ωcm) *p*- and *n*-Si can be achieved by a single SiN_x layer within a broad range of $n = 1.85$–4.07.

II. SIN_X DEPOSITION AND GROWTH MECHANISMS

The SiN_x films are deposited in a static laboratory-scale μW/RF PECVD system (Roth & Rau AG, system AK400). Figure 2 depicts a cross-section of the deposition system, which consists of two gas inlets: a gas shower at the top for injecting NH_3 or/and Ar, and a gas ring at the bottom for injecting SiH_4. The plasma is excited around quartz tubes by means of two continuous-wave magnetron microwave generators with a frequency of 2.45 GHz, introducing up to 2000 W of microwave power into the process chamber. The RF plasma is excited near the graphite substrate by means of an RF generator with a frequency of 13.56 MHz, creating a bias voltage of up to 300 V between the substrate and the ground.

Here we adapt the SiN_x growth model proposed by Smith *et al.*,[17] Kessels *et al.*[18] and Oever *et al.*[19] to discuss possible chemical reaction schemes for SiN_x growth in this work. For the gas mixture of N_2 and SiH_4, Smith *et al.*[17] and Kessels *et al.*[18] proposed that an a-Si:H-like surface layer is created by SiH_a radicals and the a-Si:H-like surface is simultaneously reacted with N radicals, leading to the formation of SiN_x. Oever *et al.*[19] studied the plasma chemistry for the gas mixture of

Downloaded 05 Mar 2013 to 150.203.45.141. All article content, except where otherwise noted, is licensed under a Creative Commons Attribution 3.0 Unported license.
See: http://creativecommons.org/licenses/by/3.0/

NH_3, SiH_4 and Ar and refined the growth model, concluding that SiN_x is formed by the direct surface reaction between the a-Si:H-like layer and NH_b radicals. We adapt the abovementioned models and refine a simple reaction scheme for SiN_x growth in this work:

(i) Gas phase dissociation:
–NH_3 is introduced into the system through the shower-head which forms part of the ceiling of the deposition chamber above the μW quartz tubes and is dissociated:

$$NH_3 + e \rightarrow NH_b + H_{3-b} + e \quad (a)$$

–SiH_4 is fed from the downstream gas ring that is between the quartz tube and RF-biased graphite substrate and is dissociated:

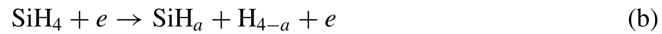

$$SiH_4 + e \rightarrow SiH_a + H_{4-a} + e \quad (b)$$

(ii) Formation/insertion:
An a-Si:H-like layer is formed on the silicon wafer by SiH_a radicals and simultaneously inserted with NH_b radicals.

(iii) Film densification by cross-linking at elevated substrate temperature to break Si–H and N–H and form Si–N:

$$\text{Si–H} + \text{N–H} \rightarrow \text{Si–N} + H_2 \quad (c)$$

Concurrently, the excessive incorporation of NH_b radicals breaks and replaces the existing Si–H bonds (at elevated substrate temperature), forming Si–N:

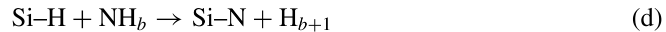

$$\text{Si–H} + NH_b \rightarrow \text{Si–N} + H_{b+1} \quad (d)$$

or otherwise, the excessive incorporation of SiH_a radicals breaks and replaces the existing N–H bonds, forming Si–N:

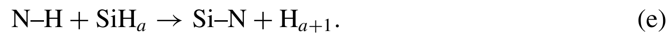

$$\text{N–H} + SiH_a \rightarrow \text{Si–N} + H_{a+1}. \quad (e)$$

III. EXPERIMENT 1: CENTRAL COMPOSITION EXPERIMENT

For the optimization of six deposition parameters, we performed the CCE that consisted of 28 different deposition conditions (parameter sets) and four additional replications of the baseline. Each set of experiments involved varying one deposition parameter while keeping the other parameters constant and at their baseline value. The relationships between SiN_x properties and individual deposition parameters are described and discussed in this section.

A. Experimental details

Table II presents the baseline and range of the deposition parameters varied in this work. It is common to have an offset between the set-point of the substrate table temperature and the actual silicon sample temperature,[9,11] so all deposition temperatures reported here refer to the actual wafer temperature measured by an external calibrated thermocouple, and not to the reactor's set-point temperature.

The lifetime samples in this experiment were *p*-type {100} FZ-Si wafers with a resistivity of 0.85 $\Omega \cdot$ cm and a thickness of 300 μm. All samples were etched in tetramethylammonium hydroxide (TMAH) at ~85 °C to remove saw damage. The *p*-Si samples were cleaned by the RCA procedure and diffused with phosphorus to getter iron and other metallic impurities.[20] The phosphorus glass was then removed in HF acid and the phosphorus-doped silicon layer was removed by etching in a 1:10 HF:HNO_3 solution. Next, all wafers were cleaned by the RCA procedure, dipped in HF to remove the native oxide, and then coated with SiN_x on both surfaces by two sequential depositions.

Downloaded 05 Mar 2013 to 150.203.45.141. All article content, except where otherwise noted, is licensed under a Creative Commons Attribution 3.0 Unported license. See: http://creativecommons.org/licenses/by/3.0/

TABLE II. Baseline and tested range of PECVD deposition parameters.

	Baseline	Range
Temperature (°C)	235	165–405
Pressure (mbar)	0.2	0.02–0.50
NH_3/SiH_4 gas flow ratio[a]	1.0	0.3–3.0
Total gas flow (sccm)[b]	60	30–240
μW plasma power (W)	500	50–1000
RF Bias voltage (V)	150	75–250

[a] Ar gas flow is kept constant at 20 sccm.
[b] sccm denotes cubic centimetre per minute at standard temperature and pressure.

The effective carrier lifetime τ_{eff} of the samples was measured using a Sinton Instruments WCT-120 operated in either transient or generalized quasi-steady-state mode, as described elsewhere.[21] The $S_{\text{eff,UL}}(\Delta n)$ can be calculated according to

$$S_{\text{eff,UL}} = \frac{w}{2}\left(\frac{1}{\tau_{\text{eff}}} - \frac{1}{\tau_{\text{bulk,intrinsic}}}\right), \tag{1}$$

Where W is the Si substrate thickness and $\tau_{\text{bulk,intrinsic}}$ is the Si intrinsic bulk lifetime parameterized by Richter *et al.*[16]

Reflectance and C-V measurements were performed on double-side-polished n-type {100} FZ-Si with a resistivity of 1.0 $\Omega \cdot$cm and a thickness of 290 μm. Metal-insulator-semiconductor (MIS) test structures were fabricated for C-V measurements. In this work, the front metal contact was formed by evaporating aluminum through a shadow mask to create circular dots of diameter ∼700 μm and thickness ∼100 nm. The rear contact was formed with a GaIn eutectic. More details on the fabrication of reflectance and C-V measurements samples, as well as the characterisation of the wavelength-dependent refractive index $n(\lambda)$ and extinction coefficient $k(\lambda)$, and the interface defect density D_{it} and effective insulator charge Q_{eff} associated with SiN_x, can be found in Ref. 15.

The FTIR transmission spectra were measured on the same samples as used for reflectance and C-V measurements, using FTIR spectrometer (Bruker Vertex 80V) with a resolution of 6 cm^{-1}. The measurement showed three distinctive absorption peaks associated with Si–N, Si–H and N–H vibrational modes about 850, 2220 and 3340 cm^{-1}, respectively.[22] The bond density [A–B], defined as the number of bonds per unit volume, can be determined by[23]

$$[\text{A–B}] = k_{\text{A–B}} \int \frac{\alpha(\omega)}{\omega} d\omega, \tag{2}$$

where $\alpha(\omega)$ is the absorption coefficient at wavenumber ω, $k_{\text{A–B}}$ is the proportionality constant in cm^{-2}. In this work, $k_{\text{A–B}}$ for Si–N, Si–H and N–H is taken from Ref. 22 having the values of 2×10^{19}, 2×10^{20} and 1.2×10^{20}, respectively.

B. Results and discussion

1. Dependence of film properties on deposition parameters

Figure 3 plots the dependence of the deposition rate, bond densities, optical and electronic properties of plasma SiN_x on the various deposition parameters. These dependencies are now described.

Deposition rate—For throughput considerations, the deposition rate by PECVD should be as high as possible. Figure 3(a) shows the effect of deposition parameters on the deposition rate. The deposition time for all conditions was 3 min, and the resulting film thickness ranged from 50 to 200 nm. We found that increasing the total gas flow within the tested range causes a threefold increase in the deposition rate. The factor increase is ∼2 for the decrease of NH_3/SiH_4 gas flow ratio and smaller (∼1.2) for the variation of other parameters.

Downloaded 05 Mar 2013 to 150.203.45.141. All article content, except where otherwise noted, is licensed under a Creative Commons Attribution 3.0 Unported license.
See: http://creativecommons.org/licenses/by/3.0/

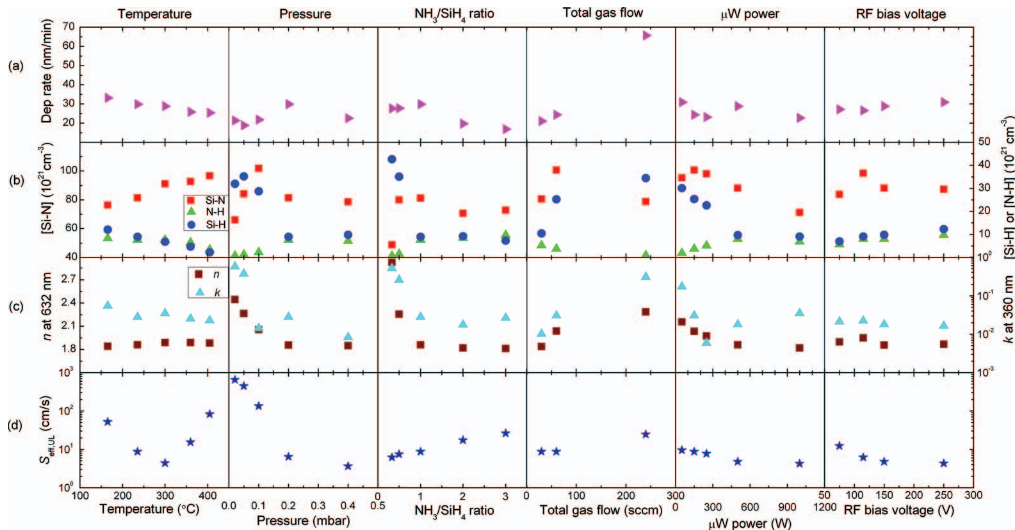

FIG. 3. Main effects plots of SiN_x (a) deposition rate; (b) chemical bond densities; (c) refractive index n at 632 nm and extinction coefficient k at 360 nm; (d) extracted surface recombination velocity $S_{eff,UL}$ at $\Delta n = 10^{15}$ cm^{-3} on FZ, 0.85 Ω cm, {100} 300 μm p-type c-Si.

***Bond densities*—**Figure 3(b) shows the influence of deposition parameters on the SiN_x chemical bond densities, namely [Si–N], [N–H] and [Si–H]. [Si–N] exhibits a peak within the tested range of all the parameters, except for temperature, for which [Si–N] increases as temperature increases. When deposition pressure, gas flow ratio and plasma power are increased, and when total gas flow is decreased, the hydrogen-bond concentrations, [N–H] and [Si–H] tend to exhibit inverse relationships, where [N–H] increases moderately and [Si–H] decreases strongly. This trend is consistent with the films becoming less Si-rich. Exceptions to this inverse correlation is that both [N–H] and [Si–H] decrease moderately as temperature increases and RF bias decreases.

Optical properties—Figure 3(c) depicts the responses of n at 632 nm and k at 360 nm to the deposition parameters. As we can see, n decreases strongly with increasing NH_3/SiH_4 gas flow ratio, μW plasma power, pressure and total gas flow, whereas it is hardly affected by the variation of deposition temperature and RF bias voltage. Moreover, Figure 4(a) and 4(b) show the dispersion relation for both the refractive index n and the extinction coefficient k. The results are consistent with those reported in other studies,[24–26] showing a decrease of n and k with increasing wavelength. As expected, SiN_x of low n ($\leq$2.0) exhibits low absorption of short-wavelength light and almost negligible absorption at wavelengths above 360 nm, implying it is better suited as the ARC in solar cells. Indeed, compared to the SiN_x of $n = 2.5$ and an equivalent passivation, the optical simulation of our previous work[15] found that the SiN_x of $n = 1.9$ would enhance the photogenerated current density by more 0.66 mA/cm^{-2} or 1.40 mA/cm^{-2} for solar cells encapsulated in glass and ethylene-vinyl acetate (EVA) or operating in air, respectively. This enhancement is due to the film's low k rather than it having the optimum n. In addition, we find that, irrespective of the variation of deposition parameters, an increase of k at 360 nm is generally accompanied by an increase of n at 632 nm, as made clearer with Figure 4(c).

***Surface passivation*—**Figure 3(d) plots $S_{eff,UL}$ of the as-deposited SiN_x. It indicates that $S_{eff,UL}$ depends strongly on deposition temperature, pressure and gas flow ratio, and slightly on total gas flow, μW plasma power and RF bias voltage. Whereas $S_{eff,UL}$ increases with increasing NH_3/SiH_4 gas flow ratio, $S_{eff,UL}$ decreases significantly as pressure increases. An optimum deposition temperature is observed at 300 °C, leading to a minimum $S_{eff,UL}$.

Figure 5 shows the injection-dependent effective lifetime $\tau_{eff}(\Delta n)$ for SiN_x-passivated p-type silicon samples. We briefly comment on how $\tau_{eff}(\Delta n)$ is affected by temperature and pressure since passivation is the most sensitive to these parameters. For reference, the Auger limit parameterized by Richter *et al.* is also plotted.[16] We note that none of the $\tau_{eff}(\Delta n)$ curves cross over except for SiN_x

Downloaded 05 Mar 2013 to 150.203.45.141. All article content, except where otherwise noted, is licensed under a Creative Commons Attribution 3.0 Unported license.
See: http://creativecommons.org/licenses/by/3.0/

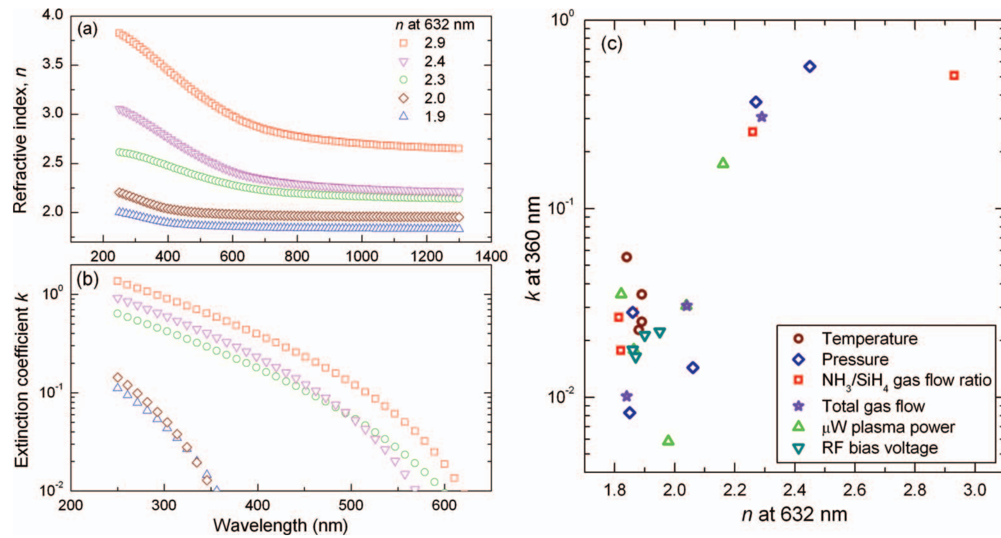

FIG. 4. Wavelength-dependent (a) refractive index n and (b) extinction coefficient k for representative SiN_x films determined from spectrophotometry measurements. The correlation between n at 632 nm and k at 360 nm is also illustrated in (c).

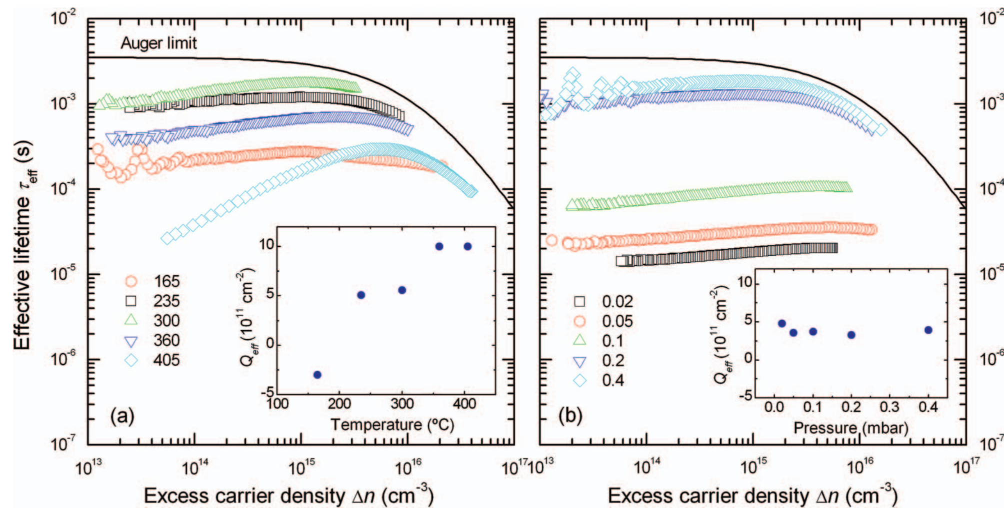

FIG. 5. Measured effective lifetime τ_{eff} as a function of excess carrier density for low resistivity p-type silicon (FZ, 0.85 Ω cm, {100} 300 μm). SiN_x is altered by the variation of (a) deposition temperature, and (b) deposition pressure. The insets demonstrate the impact of temperature and pressure on the effective insulator charge Q_{eff} in the SiN_x.

deposited at 405 °C, which has a maximum τ_{eff} at $\Delta n = 5 \times 10^{15}$ cm^{-3}. This means that we can meaningfully compare τ_{eff} (and hence $S_{\text{eff,UL}}$ as presented in Figure 2(d)) at a particular Δn, such as 1×10^{15} cm^{-3}.

Figure 5(a) shows that the shape of the $\tau_{eff}(\Delta n)$ curves diverges from the shape of the intrinsic lifetime curve as temperature increases. More specifically, there is an increasing injection dependence at low Δn, whereby τ_{eff} increases with Δn, consistent with the silicon surface being in inversion due to positive insulator charges.[27,28] With C-V measurements, we confirm this speculation. As evident in the inset of Figure 5(a), Q_{eff} increases with an increase of deposition temperature. In contrast to the temperature variation, Figure 5(b) shows that there is no change to the injection dependence of $\tau_{eff}(\Delta n)$ when pressure is varied, which correlates to a relatively constant Q_{eff}. The dependence of Q_{eff} on deposition temperature but not pressure is consistent with the insulator charge originating from thermal-assisted charge injection from the silicon substrate.[29]

Downloaded 05 Mar 2013 to 150.203.45.141. All article content, except where otherwise noted, is licensed under a Creative Commons Attribution 3.0 Unported license.
See: http://creativecommons.org/licenses/by/3.0/

Finally, the optimum deposition condition that achieves an SiN_x with low absorption and low recombination is concluded to be 300 °C, 0.2 mbar, NH_3/SiH_4/Ar gas flow at 20/20/20 sccm, μW plasma power at 500 W and RF bias voltage at 150 V. Note that even though the film deposited at 0.4 mbar provides lower $S_{eff,UL}$ than that at 0.2 mbar, we select an optimum deposition pressure of 0.2 mbar instead of 0.4 mbar because the spatial uniformity of the film was poor when deposited at 0.4 mbar. These optimum deposition conditions are utilized to examine the trade-off between optical transmission and surface passivation in Section IV.

2. Discussion on the effect of deposition parameters on film properties

We now discuss how each process parameter affects the deposition rate and chemical bond density in relation to the growth mechanism described in Section II.

Precursor gas flow ratio is commonly varied to alter SiN_x film properties as it directly tailors the partial pressure of the resultant radicals. As the NH_3/SiH_4 increases, the proportion of NH_b radicals in the reactor increases while the proportion of SiH_a radicals decreases. We therefore observe that 1) deposition rate decreases, 2) [Si–H] decreases and [N–H] increases and 3) n and k decreases.

The deposition temperature hardly affects reaction steps (i) and (ii) but causes significant change in film densification (step iii). According to Figure 3(b), both [Si–H] and [N–H] decrease as the deposition temperature increases. This behaviour is attributable to the film densification through reaction (c). As temperature increases, the film is densified through the restructuring of Si–H and N–H to form Si–N. Film densification by cross-linking at elevated temperature would also result in a decrease in film thickness, as evident in Figure 3(a).

The influence of deposition pressure and μW plasma power on the hydrogen bond densities can also be elucidated. Changing the deposition pressure and plasma power has a strong effect on the gas phase dissociation rate and the shape of the electron distribution function.[30,31] As pressure decreases, μW plasma becomes less confined near the quartz tubes and approaches the downstream SiH_4 gas injection region.[11] The decrease of pressure therefore enhances the dissociation of SiH_4 but suppresses the dissociation of NH_3, leading to an increase in [Si–H] and a decrease in [N–H]. Moreover, the excessive incorporation of SiH_a radicals (at low pressure) further reduces [N–H] through reaction (e).

Next, note that NH_3 in our reactor is injected from the top shower head and is mainly dissociated by the μW plasma power through reaction (a). This means the increase of μW plasma power enhances more dissociation of NH_3 than of SiH_4. We therefore observe that [N–H] increases with the increase of μW plasma power. Again, the excessive flux of impinging NH_b radicals (at high μW plasma power) further breaks Si–H bonds through reaction (d). These conclusions are consistent with Figure 3(b), which shows that [N–H] increases as [Si–H] decreases when either pressure or μW plasma power is increased.

Plasma power is primarily dominated by μW plasma rather than by RF plasma in a μW/RF PECVD reactor because the ion density in a μW plasma is more than one order of magnitude higher than in an RF plasma.[31] The main purpose of the RF plasma in our system is to create a bias voltage between the plasma and the substrate, thereby enhancing the flux of radicals onto the substrate surface. Based on the discussion above, we are not surprised to see in Figure 3(b) that an increase in the RF bias voltage is accompanied by a slight increase in [Si–H], [N–H] and the deposition rate.

Without sufficient information on the relative amount of gas phase consumption of a precursor, also called depletion, we cannot postulate how an increase of total gas flow causes an increase of [Si–H] and a decrease of [N–H]. Nevertheless, the strong increase of deposition rate as well as the increase of [Si–H] with increasing total gas flow further confirms that SiN_x deposition rate in our system is primarily limited by the supply of SiH_4 precursor gas or consequently by the incorporation of SiH_a radicals.

3. Correlations between SiN_x properties

a. Optical properties versus structural properties. Since an increase in refractive index n is believed to correlate to a shift in the chemical composition toward being more Si rich,[32] we plot n as a function of [Si–H]/[N–H] in Figure 6 for all deposition conditions. We can then express the results

Downloaded 05 Mar 2013 to 150.203.45.141. All article content, except where otherwise noted, is licensed under a Creative Commons Attribution 3.0 Unported license.
See: http://creativecommons.org/licenses/by/3.0/

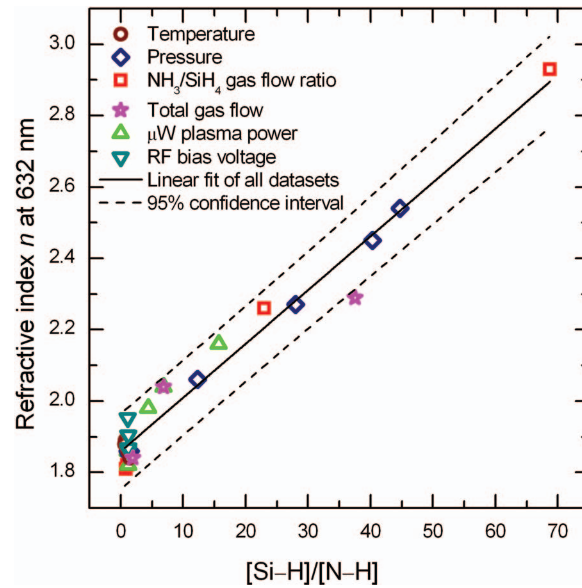

FIG. 6. Relationship between measured refractive index n at 632 nm and SiN_x bond density ratio: [Si–H]/[N–H]. The solid line is a linear best fit and the dashed lines are its 95% confidence intervals.

by the linear relationship

$$n = 0.0151(\pm 0.0006)\frac{[Si\text{–}H]}{[N\text{–}H]} + 1.86(\pm 0.01), \quad (3)$$

where the uncertainty represents the 95% confidence interval. This empirical relation indicates that, over a wide range of deposition conditions, the optical properties primarily depend on the ratio of [Si–H] to [N–H] rather than being independently correlated to [Si–N], [Si–H] and [N–H].

b. $S_{eff,UL}$ versus bond density. [Si–H] is regularly considered as a measure of surface passivation quality owing to the hypothesis that higher [Si–H] implies a higher probability that hydrogen terminates the Si dangling bonds at the SiN_x-Si interface.[9,10] Lauinger *et al.* found a clear increase in τ_{eff} with increasing n of SiN_x for p-type silicon wafers, where an increase of n corresponds to an increase of [Si–H] and a simultaneous decrease of [N–H]. This was observed both for remote PECVD SiN_x precursor gases (NH_3/SiH_4)[9] as well as direct PECVD SiN_x precursor gases ($N_2/H_2/SiH_4$).[10]

Figure 7 plots $S_{eff,UL}$ against [Si–H] for the films in our work. It shows that when the NH_3/SiH_4 gas flow ratio or RF bias voltage is varied, surface passivation improves as n increases, corresponding to an increase in [Si–H]. These results are consistent with Refs. 9 and 10. However, contrary to the trend, when other deposition parameters are varied, no consistent correlation can be established between $S_{eff,UL}$ and [Si–H]. As evident in Figure 7, $S_{eff,UL}$ keeps increasing with an increase in [Si–H] when pressure and μW plasma power are varied. More complicated behaviour is induced by varying deposition temperature whereby $S_{eff,UL}$ exhibits a minimum at [Si–H] = 7×10^{21} cm^{-3}. Clearly, there is no universal dependence of $S_{eff,UL}$ on [Si–H].

Similarly, we do not find a universal correlation between $S_{eff,UL}$ and [Si–N] for our as-deposited films. The blue squares in Figure 8 indicate that [Si–N] has little influence on the as-deposited SiN_x passivation. Figure 8 also plots $S_{eff,UL}$ against [Si–N] for the same samples after a rapid-thermal anneal (RTA) at 800 °C for 5 seconds. The results show that [Si–N] strongly affects passivation of post-RTA SiN_x, consistent with several studies which concluded that [Si–N] has a strong influence on the surface passivation after an RTA.[6,33–35] Higher [Si–N] improves the thermal stability of SiN_x passivation, attributing to lower effusion of H_2 molecules from the denser SiN_x layer into the ambient during short annealing step.[36]

Downloaded 05 Mar 2013 to 150.203.45.141. All article content, except where otherwise noted, is licensed under a Creative Commons Attribution 3.0 Unported license.
See: http://creativecommons.org/licenses/by/3.0/

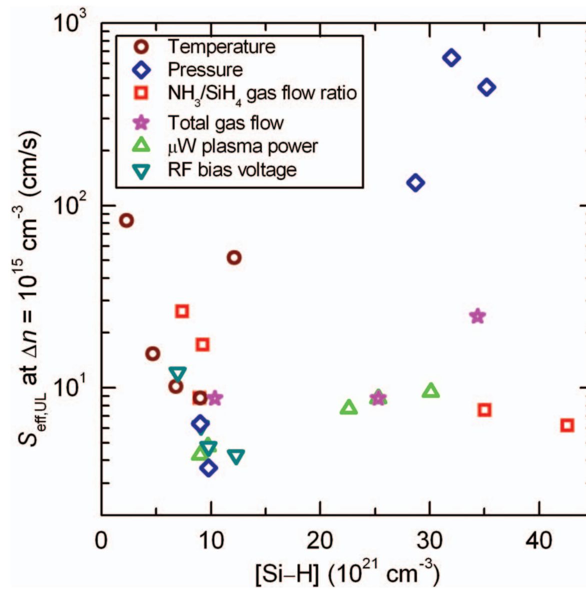

FIG. 7. $S_{\mathrm{eff,UL}}$ as a function of [Si–H] for SiN_x deposited at a variety of conditions.

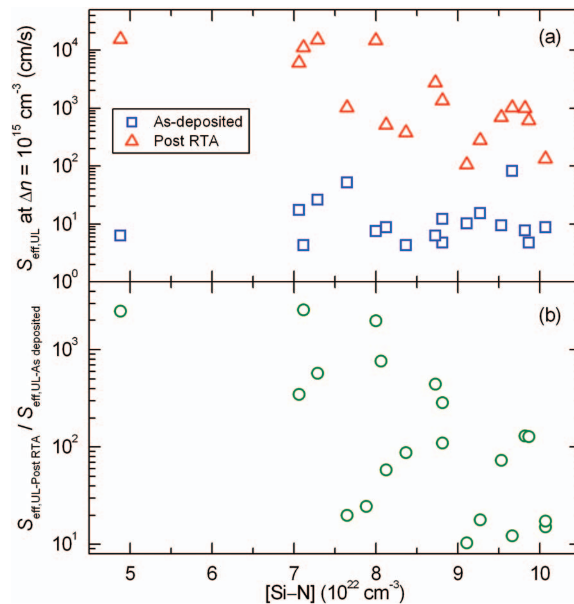

FIG. 8. (a) Extracted $S_{\mathrm{eff,UL}}$ for as-deposited and post-RTA SiN_x and (b) the ratio between $S_{\mathrm{eff,UL}}$ for as-deposited and post RTA SiN_x are plotted against [Si–N].

The universal dependence of n on [Si–H]/[N–H] and the variable dependence of $S_{\mathrm{eff,UL}}$ on [Si–H] and [Si–N] further confirms the conclusion presented in our previous work:[15] S_{eff} does not necessarily correlate to the refractive index (or stoichiometry) of SiN_x.

c. $S_{eff,UL}$ versus D_{it} and Q_{eff}. C-V measurements were performed on selected samples to determine D_{it} at midgap and Q_{eff} at flat-band. Quasi-static C-V measurements on typical SiN_x produced in this work could not be performed as they were too leaky. Hence, we treat the absolute value of D_{it} in our work with caution since D_{it} was solely determined by applying the Terman method[37] to high-frequency (HF) C-V measurements. Nevertheless, we remain confident in the conclusions derived from this study because they rely on trends, rather than absolute values of D_{it}. As shown in

Downloaded 05 Mar 2013 to 150.203.45.141. All article content, except where otherwise noted, is licensed under a Creative Commons Attribution 3.0 Unported license.
See: http://creativecommons.org/licenses/by/3.0/

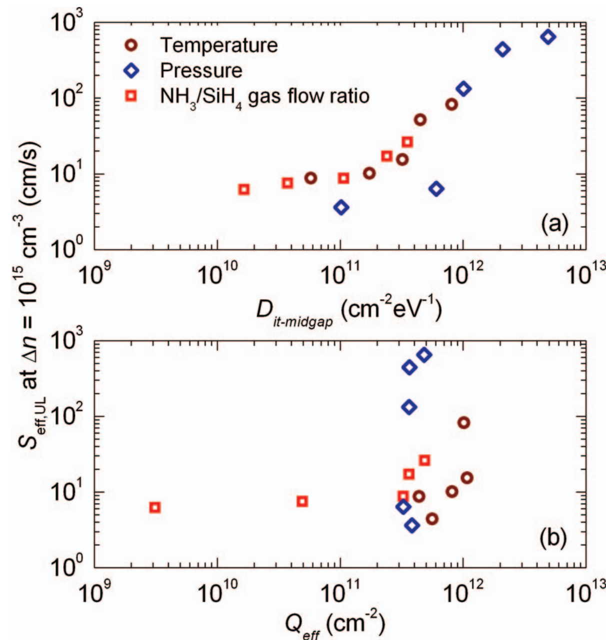

FIG. 9. Extracted $S_{\text{eff,UL}}$ as a function of (a) interface defects density D_{it} at midgap and (b) effective insulator charge Q_{eff} for the variation of deposition temperature, pressure and gas flow ratio.

Figure 9(a), we find that $S_{\text{eff,UL}}$ depends strongly on D_{it}, irrespective of the varied process parameters. As D_{it} increases over three orders of magnitude, $S_{\text{eff,UL}}$ increases by two orders of magnitude. However, $S_{\text{eff,UL}}$ shows different relationships with Q_{eff} when the SiN_x is altered by varying different deposition parameters. As evident in Figure 9(b), $S_{\text{eff,UL}}$ is almost constant as Q_{eff} increases from 3×10^9 cm^{-2} to 3×10^{11} cm^{-2}, and then exhibits two orders of magnitude variation when $Q_{\text{eff}} = 4 \times 10^{11}$ cm^{-2}. Figure 9 shows that S_{eff} at SiN_x-passivated silicon surface in this work depends primarily on interface defect density rather than charge.

IV. EXPERIMENT 2: CIRCUMVENTING THE TRADE-OFF BETWEEN OPTICAL TRANSMISSION AND SURFACE PASSIVATION

Inspired by the vastly different responses of n and S_{eff} to various deposition conditions, we now examine the challenge mentioned in Section I of developing a single SiN_x layer that circumvents the trade-off between optical transimission and surface passivation.

In relation to this goal, we note that Lauinger *et al.*[9] achieved a saturation of τ_{eff} but by very Si-rich SiN_x with n above 2.3, and Hoex *et al.*[38] presented a relatively constant $S_{\text{eff,UL}}$ within a refractive index range of 1.9–2.4, however, the $S_{\text{eff,UL}}$ associated with their SiN_x-passivated *p*-type 8.4-$\Omega \cdot$cm FZ Si substrates is relatively high (50–70 cm/s). Indeed, within a broad range of n (1.85–4.07) associated with SiN_x, a constant low $S_{\text{eff,UL}}$ on low resistivity (≤ 1.1 $\Omega \cdot$cm) Si substrates has not been achieved.

A. Experimental details

The optimized deposition conditions presented in Section III B were applied on three types of low resistivity FZ Si samples: 0.85 $\Omega \cdot$cm *p*-type, 0.45 $\Omega \cdot$cm *n*-type, and 1.10 $\Omega \cdot$cm *n*-type. The wafers received the same TMAH silicon etch, RCA clean, and double-side SiN_x deposition that were applied to the lifetime samples in Section III. Note that no gettering step was applied on *n*-Si samples, since *n*-Si has a lower sensitivity to metal contaminants than *p*-Si.[39] The $S_{\text{eff,UL}}$ at $\Delta n = 10^{15}$ cm^{-3} and n at 632 nm were characterized in accordance with the procedures described

Downloaded 05 Mar 2013 to 150.203.45.141. All article content, except where otherwise noted, is licensed under a Creative Commons Attribution 3.0 Unported license.
See: http://creativecommons.org/licenses/by/3.0/

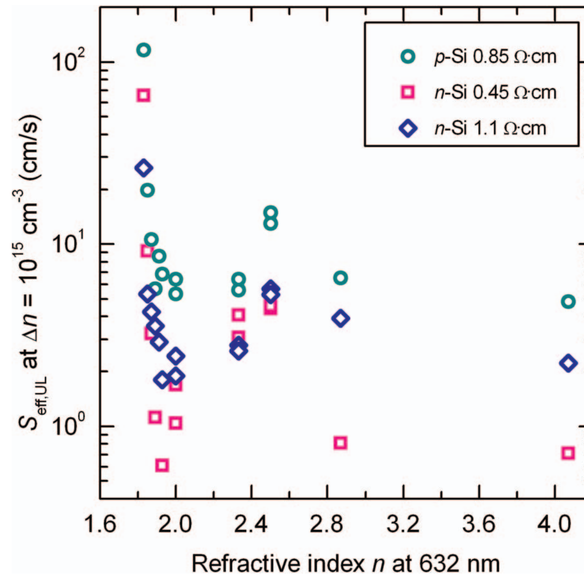

FIG. 10. Extracted $S_{eff,UL}$ for three types of FZ c-Si substrates as a function of n at 632 nm. In this experiment, only the NH_3/SiH_4 gas flow ratio was varied to alter the SiN_x properties.

in Section III A. In this experiment, the NH_3/SiH_4 gas flow ratio was then varied to obtain a broad range of n, ranging from 1.83 (sub-stoichiometric) to 4.07 (close to a-Si:H).

B. Results and discussion

The $S_{eff,UL}$ for the three types of samples is plotted against n in Figure 10. While there is no universal relationship between $S_{eff,UL}$ and n, the trend in this experiment is similar to those presented in Refs. 9 and 11 (see Figure 1). In these cases, the variation in n was achieved by varying the NH_3/SiH_4 gas flow ratio. As indicated in Figure 10, $S_{eff,UL}$ first decreases as n increases and then saturates over the range $n = 1.85$–4.07. This behaviour is seen on all three types of substrates. Note that the $S_{eff,UL}$ for 0.45 $\Omega \cdot$ cm n-Si seems typically lower than the $S_{eff,UL}$ for 1.1 $\Omega \cdot$ cm n-Si. One possible reason is that the Auger model proposed by Richter *et al.*[16] underestimates the bulk intrinsic lifetime for the 0.45 $\Omega \cdot$ cm n-Si, leading to a lower $S_{eff,UL}$. Note further that all $S_{eff,UL}$ reported in this section is by the as-deposited SiN_x.

In addition to the similar trend, we note that (i) at an equivalent value of n, our SiN_x provides a very low $S_{eff,UL}$, where the lowest $S_{eff,UL}$ is 5.3 cm/s, 0.6 cm/s and 1.8 cm/s for the aforementioned three types of Si samples and (ii) the saturation of $S_{eff,UL}$ in Refs. 9 and 11 starts at $n = 2.3$ whereas it starts at a lower n of 1.85 in this work. Overall, very low S_{effUL} is attained over a range of n where k is also low. The results of Figure 10 suggest that an appropriate deposition of SiN_x can eliminate the trade-off between ARC absorption and surface passivation. In short, solar cells that require high surface passivation need not be compromised by light absorption in the SiN_x.

V. CONCLUSION

The properties of SiN_x films synthesised by a μW/RF PECVD reactor were altered by varying the substrate temperature, pressure, NH_3/SiH_4 gas flow ratio, total gas flow, μW plasma power and RF bias voltage. After reporting on the dependence of the SiN_x film properties on the deposition parameters, we determined optimized deposition conditions that attain low absorption and low recombination. On the basis of the SiN_x growth models proposed in the literature and of our experimental results, we discussed how each process parameter affects the deposition rate and chemical bond density. By studying the correlations between the structural, optical and electrical properties, we found that for the SiN_x prepared in this work 1) $S_{eff,UL}$ does not correlate universally

Downloaded 05 Mar 2013 to 150.203.45.141. All article content, except where otherwise noted, is licensed under a Creative Commons Attribution 3.0 Unported license.
See: http://creativecommons.org/licenses/by/3.0/

with the bulk structural and optical properties such as chemical bond densities and refractive index, and 2) $S_{\mathrm{eff,UL}}$ depends primarily on the defect density at the SiN_x-Si interface rather than the insulator charge. Finally, employing the optimized deposition condition, we achieved a relatively constant and low $S_{\mathrm{eff,UL}}$ on low-resistivity ($\leq$1.1 Ωcm) *p*- and *n*-type c-Si substrates over a broad range of n = 1.85–4.07. The results demonstrate that the trade-off between optical transmission and surface passivation can be circumvented by a judicious deposition of SiN_x. Although we focus on photovoltaic applications, this study may be useful for any device for which it is desirable to maximize light transmission and surface passivation.

ACKNOWLEDGMENT

The authors would like to thank Prof. Andres Cuevas and Dr. Saul Winderbaum for valuable discussions. This work was supported by an Australian Research Council Linkage between The Australian National University and Braggone Oy under Grant LP0989593.

[1] A. G. Aberle, Solar Energy Materials and Solar Cells **65**, 239 (2001).
[2] C. Leguijt, P. Lölgen, J. A. Eikelboom, A. W. Weeber, F. M. Schuurmans, W. C. Sinke, P. F. A. Alkemade, P. M. Sarro, C. H. M. Marée, and L. A. Verhoef, Solar Energy Materials and Solar Cells **40**, 297 (1996).
[3] X. Dai and K. R. McIntosh, in *Proc. 35th IEEE PVSC*, Proc. 35th IEEE PVSC, 2010, pp. 3205.
[4] B. Gorowitz, T. B. Gorczyca, and R. J. Saia, Solid State Technology **28**, 197 (1985).
[5] Z. Chen, A. Rohatgi, R. O. Bell, and J. P. Kalejs, Applied Physics Letters **65**, 2078 (1994).
[6] A. W. Weeber, H. C. Rieffe, M. J. A. A. Goris, J. Hong, W. M. M. Kessels, M. C. M. van de Sanden, and W. J. Soppe, in *Photovoltaic Energy Conversion, 2003. Proceedings of 3rd World Conference on*, 2003, p. 1131.
[7] H. F. W. Dekkers, L. Carnel, and G. Beaucarne, Applied Physics Letters **89**, 013508 (2006).
[8] J. Hong, W. M. M. Kessels, W. J. Soppe, A. W. Weeber, W. M. Arnoldbik, and M. C. M. v. d. Sanden, Journal of Vacuum Science & Technology B: Microelectronics and Nanometer Structures **21**, 2123 (2003).
[9] T. Lauinger, J. Moschner, A. G. Aberle, and R. Hezel, Journal of Vacuum Science & Technology A: Vacuum, Surfaces, and Films **16**, 530 (1998).
[10] H. Mäckel and R. Lüdemann, Journal of Applied Physics **92**, 2602 (2002).
[11] J. D. Moschner, J. Henze, J. Schmidt, and R. Hezel, Progress in Photovoltaics: Research and Applications **12**, 21 (2004).
[12] J. F. Lelièvre, E. Fourmond, A. Kaminski, O. Palais, D. Ballutaud, and M. Lemiti, Solar Energy Materials and Solar Cells **93**, 1281 (2009).
[13] S. D. Gupta, B. Hoex, L. Fen, T. Mueller, and A. G. Aberle, in *Photovoltaic Specialists Conference (PVSC), 2011 37th IEEE*, 2011, p. 001421.
[14] J. Schmidt and M. Kerr, Solar Energy Materials and Solar Cells **65**, 585 (2001).
[15] Y. Wan, K. R. McIntosh, A. F. Thomson, and A. Cuevas, Photovoltaics, IEEE Journal of **PP**, 1 (2012).
[16] A. Richter, S. W. Glunz, F. Werner, J. Schmidt, and A. Cuevas, Physical Review B **86**, 165202 (2012).
[17] D. L. Smith, A. S. Alimonda, and F. J. v. Preissig, Journal of Vacuum Science & Technology B: Microelectronics and Nanometer Structures **8**, 551 (1990).
[18] W. M. M. Kessels, F. J. H. v. Assche, J. Hong, D. C. Schram, and M. C. M. v. d. Sanden, Journal of Vacuum Science & Technology A: Vacuum, Surfaces, and Films **22**, 96 (2004).
[19] P. J. v. d. Oever, J. H. v. Helden, J. L. v. Hemmen, R. Engeln, D. C. Schram, M. C. M. v. d. Sanden, and W. M. M. Kessels, Journal of Applied Physics **100**, 093303 (2006).
[20] S. P. Phang and D. Macdonald, Journal of Applied Physics **109**, 073521 (2011).
[21] R. A. Sinton and A. Cuevas, Applied Physics Letters **69**, 2510 (1996).
[22] F. Giorgis, F. Giuliani, C. F. Pirri, E. Tresso, C. Summonte, R. Rizzoli, R. Galloni, A. Desalvo, and P. Rava, Philosophical Magazine Part B **77**, 925 (1998).
[23] M. Cardona, physica status solidi (b) **118**, 463 (1983).
[24] P. Doshi, G. E. Jellison, and A. Rohatgi, Appl. Opt. **36**, 7826 (1997).
[25] S. Duttagupta, F. Ma, B. Hoex, T. Mueller, and A. G. Aberle, Energy Procedia **15**, 78 (2012).
[26] M. H. Kang, K. Ryu, A. Upadhyaya, and A. Rohatgi, (John Wiley and Sons, Ltd.), p. n/a.
[27] A. G. Aberle, T. Lauinger, J. Schmidt, and R. Hezel, Applied Physics Letters **66**, 2828 (1995).
[28] M. J. Kerr and A. Cuevas, Semiconductor Science and Technology **17**, 166 (2002).
[29] J. R. Elmiger and M. Kunst, Applied Physics Letters **69**, 517 (1996).
[30] G. Turban, Y. Catherine, and B. Grolleau, Thin Solid Films **67**, 309 (1980).
[31] L. Martinu and D. Poitras, Journal of Vacuum Science & Technology A: Vacuum, Surfaces, and Films **18**, 2619 (2000).
[32] J. Robertson, Philosophical Magazine Part B **63**, 47 (1991).
[33] A. W. Weeber, H. C. Rieffe, I. G. Romijn, W. C. Sinke, and W. J. Soppe, in *Photovoltaic Specialists Conference, 2005. Conference Record of the Thirty-first IEEE*, 2005, p. 1043.
[34] A. Cuevas, C. Florence, T. Jason, M. Helmut, W. Saul, and R. Kristin, in *Photovoltaic Energy Conversion, Conference Record of the 2006 IEEE 4th World Conference on*, 2006, p. 1148.

Downloaded 05 Mar 2013 to 150.203.45.141. All article content, except where otherwise noted, is licensed under a Creative Commons Attribution 3.0 Unported license.
See: http://creativecommons.org/licenses/by/3.0/

[35] F. Chen, I. Romijn, A. Weeber, J. Tan, B. Hallam, and J. Cotter, in *22nd European Photovoltaic Solar Energy Conference*, Milan, Italy, 2007, p. 1053.
[36] H. F. W. Dekkers, G. Beaucarne, M. Hiller, H. Charifi, and A. Slaoui, Applied Physics Letters **89**, 211914 (2006).
[37] L. M. Terman, Solid-State Electronics **5**, 285 (1962).
[38] B. Hoex, A. J. M. van Erven, R. C. M. Bosch, W. T. M. Stals, M. D. Bijker, P. J. van den Oever, W. M. M. Kessels, and M. C. M. van de Sanden, Progress in Photovoltaics: Research and Applications **13**, 705 (2005).
[39] D. Macdonald and L. J. Geerligs, Applied Physics Letters **85**, 4061 (2004).

Downloaded 05 Mar 2013 to 150.203.45.141. All article content, except where otherwise noted, is licensed under a Creative Commons Attribution 3.0 Unported license.
See: http://creativecommons.org/licenses/by/3.0/